



**HAL**  
open science

## Creep investigations on adhesively bonded fasteners developed for offshore steel structures

Ethel Djeumen, Sylvain Chataigner, Romain Créac'Hcadec, Quentin Sourisseau, Marie-Odette Quemere, Jean-Philippe Court, Firas Sayed

► **To cite this version:**

Ethel Djeumen, Sylvain Chataigner, Romain Créac'Hcadec, Quentin Sourisseau, Marie-Odette Quemere, et al.. Creep investigations on adhesively bonded fasteners developed for offshore steel structures. Marine Structures, 2020, 69, 14 p. 10.1016/j.marstruc.2019.102660 . hal-02431022

**HAL Id: hal-02431022**

**<https://hal.science/hal-02431022>**

Submitted on 7 Jun 2021

**HAL** is a multi-disciplinary open access archive for the deposit and dissemination of scientific research documents, whether they are published or not. The documents may come from teaching and research institutions in France or abroad, or from public or private research centers.

L'archive ouverte pluridisciplinaire **HAL**, est destinée au dépôt et à la diffusion de documents scientifiques de niveau recherche, publiés ou non, émanant des établissements d'enseignement et de recherche français ou étrangers, des laboratoires publics ou privés.

1 **Creep investigations on adhesively bonded fasteners developed for**  
2 **offshore steel structures**

3 E. Djeumen<sup>1</sup>, S. Chataigner<sup>1</sup>, R. Créac'hcadec<sup>2</sup>, Q. Sourisseau<sup>1</sup>, M.O. Quéméré<sup>3</sup>, J.P. Court<sup>3</sup>,  
4 F. Sayed<sup>3</sup>

5 <sup>1</sup>IFSTTAR, Laboratoire Structure Métallique à Câble (SMC), Département MAST, Route de  
6 Bouaye, 44 344 Bouguenais

7 Corresponding author: [sylvain.chataigner@ifsttar.fr](mailto:sylvain.chataigner@ifsttar.fr)

8 <sup>2</sup>ENSTA Bretagne, UMR CNRS 6027, IRDL, F-29200 Brest, France

9 <sup>3</sup>COLD PAD, 130 Rue de Lourmel, 75015 Paris

10

11

12 **Abstract**

13 Fastening or reinforcement onto an existing steel structure may create constraints such as the  
14 use of hot works (i.e. welding) or loss of weathertightness (i.e. drilling holes and bolting). In  
15 order to limit these constraints, there may be a strong interest in using adhesively bonded  
16 fasteners. Such a solution requires however strong justification especially regarding long-term  
17 properties. This paper presents the results of experimental and numerical investigations  
18 realized on the creep behaviour of such bonded fasteners developed for offshore steel  
19 structures. Experimental investigations were conducted at room temperature following a  
20 precise and repeatable implementation protocol. The results of the various investigations  
21 revealed a non-linear evolution of creep displacements according to a Burger law. Numerical  
22 modelling has therefore been developed on the basis of Burger's law. A preliminary static study  
23 aimed at validating the geometric model and analyzing the initial stress state in the adhesive.  
24 The creep study was then carried out to compare numerical results to experimental ones.  
25 Although additional investigations are needed, numerically determined creep displacements  
26 demonstrated a good consistency with the experimental investigations.

27

28 **Keywords:** Creep, Adhesive bonding, Fastener, Modelling, Experimental investigations.

29

30

## 31 1. Introduction

32 Steel structures in service, especially in harsh environments, may be locally affected by fatigue  
33 and corrosion and may therefore need reinforcement or repair. In addition, most often there is  
34 some need during the structure service life to connect additional equipment, secondary  
35 structures or distribution systems. In the case of steel structures, this is carried out using bolted  
36 or welded assembly that may be detrimental regarding operation issues (e.g. hot works such  
37 as welding in an explosive environment) and may induce heavy on-site constraints for the  
38 structure exploitation. In regards with these issues, adhesive bonding solution may appear as  
39 a good solution, provided that the robustness and the durability of the assembly is confirmed.  
40 The firm Cold Pad, Paris, France is currently developing an adhesively bonded fastener to  
41 provide such a solution for offshore applications [1]. They are also developing an overall  
42 solution that includes an application disposal ensuring precise control of the adhesive joint  
43 quality during application, and water tightness of the joint to prevent any durability issue linked  
44 to wet environment [2] (Figure 1).

45 Durability of adhesively bonded joint covers several damage mechanisms that may be induced  
46 by the environment or the applied load [3]. In the case of the studied bonded fasteners, as  
47 water tightness is ensured, creep and fatigue appear the main durability issues that needs to  
48 be addressed [4-5]. It was decided to first investigate creep behaviour without taking into  
49 account fatigue creep phenomena that may arise [6]. Most often, experimental creep studies  
50 of adhesively bonded joints are carried out at the scale of the adhesive alone [7]. Yet, it is well  
51 known that stress states at full scale of the bonded assembly are strongly non-uniform [8]. It  
52 was thus decided for this study to realize experimental investigations at the scale of the bonded  
53 fastener, and to develop in parallel a finite element model. This model takes into account the  
54 creep behaviour of the adhesive in order to be able to visualize the internal stress state of the  
55 joint during the test and to compare some local measurements with numerical results.

56 A short literature review on the main available creep models will first be introduced. Then, the  
57 developed experimental investigations will be described. The aim was to investigate the two

58 main loadings that may encounter the developed bonded fasteners: tension loading  
59 perpendicular to the bonded surface, and shear loading parallel to the bonded surface. After a  
60 presentation of the obtained results, the developed finite model will be introduced and the  
61 obtained results analysed. The last part will be dedicated to the comparison of the numerical  
62 model with the experimental results.

63

## 64 **2. Literature review on creep modelling**

65 Creep is the response of a material to a constant stress [9]. The creep is characterized by  
66 three stages as illustrated in Figure 2 delimited by the evolution of the strain rate: primary stage  
67 with a decreasing strain rate, secondary stage with a constant strain rate and tertiary stage  
68 with an increasing of strain rate until the failure.

69 Mathematically, the creep strain  $\varepsilon(t)$  should be noted in the form of equation (1) [9].

$$70 \quad \varepsilon(t) = \sigma^0 J(t, T, \sigma^0) \quad (1)$$

71  $J$  being creep compliance that depends mainly on time  $t$ , temperature  $T$  and applied stress  $\sigma^0$   
72 [10].

73 Two main categories of modelling strategies exist in the literature: the empirical or semi-  
74 empirical approaches and the rheological ones. Main models will be described in the two  
75 following parts.

### 76 *2.1. Semi-empirical models*

77 Various mathematical forms have been empirically proposed to describe the mechanical  
78 behaviour under creep loading. The simplest is a linear function of the stress but non-linear  
79 (logarithmic for example) when depending on time. The most commonly used expression of  
80 creep compliance is a power law given by equation (2) [11-13].

$$81 \quad J(t) = J_0 + J_1 t^n \quad (2)$$

82

83 where ( $J_0$ ;  $J_1$ ;  $n$ ) are material parameters of the model. Other empirical models exist. An  
84 example is that of Bailey Norton which allows to take into account the nonlinear behaviour and  
85 the influence of the temperature. The expression of creep compliance is then given by equation  
86 (3) [9].

$$87 \quad J(t, \sigma, T) = C_0 \sigma^{C_1} t^{C_2} \exp(-C_T/T) \quad (3)$$

88  
89 ( $C_0; C_1; C_2; C_T$ ) being the material constants of the model.

90  
91 Another example of a nonlinear model is given by equations (4) [13]. This empirical model is  
92 based on the fact that increasing the stress level has the effect of reducing the relaxation time  
93  $t_0$ .

$$94 \quad J(t, \sigma) = J_0 \exp(-t/t_0)^m \quad (4)$$
$$95 \quad t_0 = A \exp(-\alpha \sigma_0^2)^m$$

96  
97 where ( $A$ ;  $\alpha$ ) are material parameters of the model.

## 98 99 2.2. Rheological Models

100  
101 The creep behaviour can also be described by a rheological approach with basic mechanical  
102 systems. Figure 3.a and Figure 3.b below show the rheological formulation and the  
103 representation of elasticity by the spring ( $E$ ) and the viscosity by the dashpot ( $\eta$ ), where  $\sigma$  is  
104 the stress in the system and  $\epsilon$  is the strain. Kelvin-Voigt's model combines spring and dashpot  
105 in parallel (Figure 3.c). It is a solid model at infinity [9]. The expression of creep compliance is  
106 given by equation (5).

$$107 \quad J(t) = 1/E [1 - \exp(-E/\eta \cdot t)] \quad (5)$$

108  
109  $\eta/E$  being the characteristic time of the model.

110 The creep response of a material for the Kelvin-Voigt model is shown in Figure 3.c below. We  
111 find that this model does not predict the instantaneous elasticity ( $J(0) = 0$ ). It only illustrates  
112 the first stage of creep.

113  
114 The Maxwell model itself consists of a spring and a dashpot mounted in series (Figure 3.d). It  
115 is a fluid model at infinity [9]. The expression of creep compliance is:

$$116 \quad J(t) = 1/E + t/\eta \quad (6)$$

117

118 where  $E$  is the Young's modulus and  $\eta$  the viscous parameters.

119 The creep response of a material for the Maxwell model is shown in Figure 3.d below. This  
120 model brings out the second stage of creep.

121 The Burger model is obtained by associating in series the Kelvin-Voigt model and the Maxwell  
122 model. This model shows the first two stages of creep (Figure 3.e). Creep compliance is  
123 obtained by summing up the compliances of the Kelvin-Voigt and Maxwell models (equation  
124 7) [4].

$$125 \quad J(t) = 1/E_1 + t/\eta_1 + 1/E_2 [1 - \exp(-E_2 / \eta_2 \cdot t)] \quad (7)$$

126

127 where  $(E_1; E_2)$  are the spring parameters and  $(\eta_1; \eta_2)$  the viscous ones.

128

### 129 2.3. 3D creep

130

131 The concept of creep can be generalized in 3D. The creep compliance  $\mathbf{J}$  is in this case a tensor  
132 of order 4. The response to 3D creep is of the form of equation (8) [9].

$$133 \quad \boldsymbol{\varepsilon}(t) = \mathbf{J} : \boldsymbol{\sigma}^0 \quad (8)$$

134

135 In the hypothesis of an isotropic linear viscoelastic behaviour, the relation (8) takes the form of  
136 equation (9) [9].

$$137 \quad \boldsymbol{\varepsilon}(t) = (1 + \nu(t)) J(t) \boldsymbol{\sigma}^0 - \nu(t) J(t) \text{tr}(\boldsymbol{\sigma}^0) \mathbf{I} \quad (9)$$

138

139 where  $J(t)$  and  $\nu(t)$  are respectively the uniaxial creep compliance and the Poisson's ratio  
140 determined from a simple tensile creep experiment carried out in any direction. In general, the

141 Poisson's ratio doesn't depend on time,  $\nu(t) = \nu$  [14].

142 It was decided to focus in the presented work on the first two stages of creep relying on the  
143 use of the presented Burger rheological model and to make a hypothesis of an isotropic  
144 behaviour.

### 145 **3. Experimental investigations on adhesively bonded fasteners.**

146  
147 The led investigations have been carried out at full scale of the developed adhesively bonded  
148 fasteners. Preliminary quasi-static tests have been realized to determine the ultimate  
149 capacities of the assemblies for two solicitations: tension loading (perpendicular to the bonded  
150 surface) and shear loading (parallel to the bonded surface). Then, creep investigations have  
151 been carried out for the two solicitations.

#### 152 *3.1. Description of the tested specimens*

153 The tested steel fasteners have been developed by Cold Pad, Paris, France and are called C-  
154 Claw<sub>TM</sub> [1]. Two different fasteners were tested: one dedicated to a shear dominant solicitation  
155 mode: fastener S, and the other one dedicated to a tension dominant solicitation mode:  
156 fastener T. A photo of both studied fasteners T and S is given in Figure 4. Both consists in a  
157 circular steel plate with a connected steel stud (i.e. thread rod). The circular steel plate  
158 geometry has been adapted to the applied load.

159 These fasteners have been bonded to square 20 mm thick steel plates. The studied adhesive  
160 is a commercial methacrylate adhesive whose main characteristics are given in table 1 where  
161  $E$  are respectively the Young's modulus,  $RT$ , the Tensile strength and  $Tg$ , the Glass transition  
162 temperature. The surface preparation has been carried out in agreement with the adhesive  
163 specifications.

164 Two specific test settings have been developed to be able to apply the selected solicitation  
165 using a hydraulic test machine both in quasi-static and creep situations (Figure 5).

166

167

168           3.2.    *Tension test protocol*

169   The tensile test was performed with the tensile fastener bonded to a 20mm thick plate bolted  
170   to a tensile frame. The assembly was connected to a hydraulic test machine via the tensile  
171   frame for the upper grip and a connection sleeve for the lower grip as shown in Figure 6.  
172   Alignment of the frame and the connection sleeve was essential to macroscopically ensure a  
173   load in pure tension and limit the cleavage of the assembly. The loading was applied at a speed  
174   of 1.2 kN/s. Three LVDT sensors placed at 120° measured out-of-plane displacements during  
175   the test as shown in Figure 6. It allowed obtaining indication on the symmetry of the test, but  
176   also on the long-term behaviour during creep tests.

177  
178           3.3.    *Shear test protocol*

179   The shear test in principle was identical to that in tension. The shear fastener was bonded to  
180   a 20mm thick plate bolted to the shear frame. Figure 7 presents the assembly used for the  
181   realization of shear tests. The assembly was connected to the loading machine via a shear  
182   frame for the upper grip and the connection plate for the lower grip. For the same reason as in  
183   tension, the alignment of the shear frame and the connection plate had to be achieved to limit  
184   cleavage of the assembly. Loading was done at the same speed of 1.2 kN/s. A sensor makes  
185   it possible to measure the displacement in the plane (sensor 1) and three sensors placed at  
186   120° made it possible to measure the out-of-plane displacement (sensors 2, 3, 4) during the  
187   test as illustrated in Figure 7.

188  
189           3.4.    *Preliminary quasi static investigations*

190   For both solicitations, preliminary quasi static investigations up to failure were carried out to  
191   determine the ultimate capacities of the bonded assemblies. Three tests for each configuration  
192   were realized at 25 °C. Similar capacities were obtained for both configurations around 100  
193   kN, and the obtained variations were 4 and 12 % for respectively the shear and tension tests.  
194   The results allowed obtaining ultimate capacities used to settle the applied load during the

195 creep investigations. The average ultimate capacity in tension will be denoted T and the one  
196 in shear will be denoted S.

197  
198 *3.5. Results of tensile creep tests*

199 It was decided to carry out two creep tests in tension at an applied load corresponding  
200 respectively to 59 % and 69 % of the ultimate load capacity T. Figure 8.a and Figure 8.b shows  
201 the evolution of the experimentally measured out-of-plane displacements for the tensile creep  
202 tests for these two respective loads. The 59 % test lasted 10 hours 36 minutes before being  
203 interrupted. Only the first two creep stages are visible in Figure 8. The 69 % test lasted 3 hours  
204 16 minutes before failure occurred. The displacement measured by the sensor 3 made it  
205 possible to distinguish the three creep stages. The first stage lasted about 30 minutes and **the**  
206 **second stage 2 hours** before the final stage started (stage 3). Interestingly, in both cases, it  
207 can be noticed that measured displacements are highly asymmetric. There seems to be a  
208 localisation of the phenomenon. Obviously, creep phenomenon was more pronounced when  
209 the applied load is higher.

210  
211 *3.6. Results of creep shear tests*

212  
213 The shear creep tests were carried out for closed values of the percentage of the applied load  
214 in comparison with the ultimate load capacity: 59 and 67 % of the ultimate load capacity in  
215 shear S. Figure 9.a and Figure 9.b shows the results of the measured displacements for these  
216 two shear creep tests. Only two displacements are presented: sensor 1 represents the  
217 displacement in the direction parallel to the bonded surface, sensor 3 represents the peel  
218 displacement in the extremity of the assembly. The sensors 2 and 4 measured very low  
219 displacements and are therefore not plotted here.

220 The test at 59 % of the ultimate load capacity in shear S lasted 15 hours before being  
221 interrupted. Only the first two creep stages were measured. The in-plane displacement of the  
222 shear fastener measured by the sensor 1 was 221  $\mu\text{m}$  (5 times the static displacement during

223 the loading). The out-of-plane displacement of the fastener measured by the sensor 3 has  
224 reached 74  $\mu\text{m}$  (6 times the static displacement). Only the first two stages were measured.

225 The test at 67 % of the ultimate load capacity  $S$  lasted 25 minutes before failure of the assembly  
226 for an in-plane displacement measured by sensor 1 equal to 380  $\mu\text{m}$  and an out-of-plane  
227 displacement (sensor 3) of 230  $\mu\text{m}$ . The three creep stages were measured in this case.

## 228 **4. Modelling of the tests**

### 230 *4.1. Development of models*

232 For both solicitations, finite element analyses were carried out using the commercial Software  
233 Abaqus, Paris, France.

234 To model the tensile test, it was possible to use a 2D axisymmetric model (Figure 10) by  
235 making the assumption that the bolted zones were sufficiently far from the adhesive layer. To  
236 further simplify, the assumption was made that the support parts (tensile frame, sleeve) were  
237 dimensionally stable and did not need to be taken into account in the model. The behaviours  
238 of the adhesive, the plate and the tensile fastener were assumed to be isotropic linear elastic.

239 In a bonded assembly, the accuracy of the stress state is dependent on the number of  
240 elements in the thickness of the adhesive [15]. It was thus decided to lead a preliminar study  
241 on the influence of the mesh on the obtained stress states for each studied configuration.  
242 Linear rectangular elements were used and chosen as close as possible to square elements.  
243 "Cleaned" edges as advised in [15] were modelled for the free end of the adhesive layer to  
244 decrease singularity effects in this location. The mesh size was kept constant for the whole  
245 model and controlled by the numbers of elements in the adhesive layer. The convergence  
246 study investigated 3, 6 and 12 elements in the thickness mesh. The results in the case of the  
247 2D modelling of the tensile test are given in figure 11. It can be observed that stress states in  
248 the middle of the adhesive are similar for the 6 and 12 elements in the thickness configurations.

249 Consequently, 6 linear rectangular elements were used in the thickness of the adhesive to  
250 obtain representative results while limiting the needed calculation time.

251 In order to validate the hypothesis made for the 2D axisymmetric model, a 3D model presented  
252 in Figure 12 was also realized. Similar mesh configuration to the 2D model were adopted. The  
253 two planes of symmetry of the problem allowed reducing the model to only a quarter of the  
254 global geometry (Figure 10).

255 On the whole, the assumptions made for the shear calculation were the same as in tension.  
256 Only the plate, the adhesive and the non-cylindrical part of the fastener were modelled. It was  
257 necessary to use a 3D model as the loading was not axisymmetric. The 3D shear model had  
258 a plane of symmetry shown in Figure 13. This plane of symmetry made it possible to model  
259 only half of the total geometry. The boundary conditions used for the shear calculation are  
260 shown in Figure 13.

261

#### 262 4.2. Study of stress distribution and 2D / 3D comparison

263 As preliminary investigations, the modelling was realized in elastic situation taking into account  
264 the obtained average quasi static ultimate capacities for both solicitations. For both cases,  
265 several stresses are studied: shear (SXY) and peel stresses (SYY), von Mises equivalent  
266 stress (SVM) and hydrostatic pressure ( $p$ ).

267 For the case of tension load, Figure 14 presents the normalised stress states (in comparison  
268 with the ultimate von Mises stress) along the normalised bonded length (on one radius, as the  
269 assembly is axisymmetric). For each studied stress component, three positions in the adhesive  
270 layer were studied: top of the adhesive closed to the fastener, middle of the adhesive and  
271 bottom of the adhesive closed to the steel plate.

272 It can be observed that the position in the adhesive thickness does not seem to have a great  
273 influence on the studied results. In addition, it can be highlighted that although the  
274 macroscopically applied load is a tensile stress, the stress state in the adhesive is not simple.

275 The multiaxial stress state in the adhesive is explained by the non-regular geometry of the  
276 tensile fastener. In the middle of the adhesive layer, there seems to be mostly tensile stresses  
277 in the adhesive, whereas, far from the centre, shear stress seems to be predominant.  
278 Interestingly, the geometry of C-Claw<sub>TM</sub> seems to avoid obtaining stress concentrations at the  
279 free edges of the assembly in tension.

280 In order to verify the 2D assumption, a comparison was carried out between 2D results and  
281 3D results. In the 3D model, as the model is not axisymmetric anymore, two directions were  
282 studied (Figure 15 a). The results in 2D and 3D are very similar as shown in Figure 15 b, thus  
283 validating the assumptions made for the calculation in 2D.

284 For the case of the shear load, the results in terms of normalised stresses (relatively with the  
285 maximum von Mises stress) along the main diameter (oriented along the load axis) are given  
286 in Figure 16. Again, there is no large difference between the different studied adhesive  
287 thickness locations. The obtained stress state is also multiaxial with a non-uniform shear stress  
288 and an equilibrated peel stress profiles (due to the applied moment). Interestingly, it can also  
289 be checked that the geometry of C-Claw<sub>TM</sub> seems to avoid obtaining stress concentrations at  
290 the free edges of the assembly in shear.

#### 291 4.3. *Determination of creep parameters from measured displacements*

292 The creep law used to model the creep behaviour of the adhesive is Burger's law. This is the  
293 most used law for polymeric materials. Moreover, the observation of the evolution of  
294 displacements measured during creep tests seems to be rather close to the Burger model.

295 The identification of Burger's law parameters is done by hand for both assemblies assuming a  
296 uniaxial tensile stress for tensile creep test and uniaxial shear stress for shear creep test. The  
297 used stress for identification is the average tensile and shear stress along the adhesive  
298 respectively for tensile and shear creep test. The obtained parameters are given in the table  
299 2. The model is applied to the adhesive material in Abaqus software using a subroutine  
300 especially developed for the application.

#### 301           4.4.   *Study of the von Mises stress distribution during creep*

302 Figure 17 illustrates the phenomenon of stress redistribution for the tensile model that occurs  
303 due to the initial non-uniform distribution of stresses along the adhesive. Figure 17 b represents  
304 the von Mises stress state along the radius of the bonded surface during creep. Figure 17 c  
305 shows the average tensile displacement during creep and the localization of the three studied  
306 time moments. Interestingly, the stress redistribution with time allows decreasing stress  
307 concentration effect, and more particularly the ultimate von Mises stress by 23 %.

308 Figure 18 illustrates the phenomenon of stress redistribution in the case of the shear test. This  
309 redistribution was less pronounced in shear than in tension because, initially, the distribution  
310 is more uniform in shear than in tension. The maximum von Mises stress after creep was  
311 reduced by 14%.

### 312           **5. Comparison of measured displacements / model displacement**

#### 313 314           5.1.   *Tension load*

315 Figure 19 shows the comparison between the mean creep displacement measured during the  
316 tests (mean displacement of the three sensors placed at 120°) and the creep displacement  
317 determined numerically for the two tested loads. The differences between experimental and  
318 numerical curves were negligible. It was possible to model with good accuracy the creep  
319 displacements for the first two stages at different levels of loads. Yet, it must be highlighted  
320 that it was necessary to modify Burger's parameters and that they seem consequently to be  
321 dependent on the load level.

#### 322 323           5.2.   *Shear load*

324 Figures 20 and 21 represent the comparison of experimental and numerical results of out-of-  
325 plane (sensor 3, Figure 20.b and Figure 21.b) and in-plane (sensor 1, Figure 20.a and Figure  
326 21.a) displacements for shear creep tests with the two studied load levels. The difference  
327 between the experimental curve and the numerical one for the creep displacement in the plane  
328 was negligible (Figure 20.a and Figure 21.a). Again, the used modelling approach seems to

329 be well suited to the modelling of the creep of the assembly. Similarly, to the tension case, the  
330 Burger parameters had to be modified indicating a dependency of these parameters to the  
331 applied load. As far as out-of-plane displacements were concerned, there seemed to be large  
332 differences between the experimental measures and the model (Figure 20.b and Figure 21.b).  
333 There is therefore a need to improve the use model especially regarding isotropy hypothesis.

### 334 **5.3. Discussion on future developments**

335 The presented work allowed settling a modelling approach of the creep behaviour of adhesively  
336 bonded fasteners and checking its adequacy for the first two stages of creep. On the basis of  
337 the presented work, additional experimental investigations will be carried out with different load  
338 levels for both configurations to assess the load dependency of the creep model parameters.  
339 This should also improve the proposed modelling approach taking into account for example  
340 anisotropy. Additional developments will then be carried out to include stage 3 modelling  
341 approach in order to fully understand creep mechanisms and propose design guidelines and  
342 state indicators of such technical solution.

## 343 **6. Conclusions**

344  
345 If the interest in using adhesively bonded fasteners exists for steel structures, there have been  
346 few studies presenting experimental investigations led at the scale of the fastener. The  
347 presented study is one of those and aimed at initiating investigations on the creep behaviour  
348 of such fastener.

349 The presented work investigated C-Claw<sup>TM</sup> solution developed by Cold Pad, Paris, France with  
350 a methacrylate adhesive system [1]. After a specific development on the test protocol, two  
351 main load situations that may be encountered on site were studied: tension and shear.  
352 Preliminary investigations allowed determining the ultimate capacities and the repeatability of  
353 the assembly process.

354 A modelling work was then carried out using commercial finite element software Abaqus, Paris,  
355 France with specific development dedicated to the integration of Burger's isotropic creep

356 model. This work aimed at first in analysing the initial stress state in both load situations  
357 (tension and shear). It was proved that for both cases, stress is not uniform and is actually  
358 composed of peel and shear components (or pressure and von Mises stresses) depending on  
359 the fastener's geometry and the applied load.

360 Creep modelling was then carried out with an initial determination of Burger's parameters from  
361 the obtained experimental results. A good agreement was obtained between the measured  
362 average main displacements (out of plane in the case of tension and in plane in the case of  
363 shear), and the numerically obtained ones provided that Burger's parameters were dependent  
364 on the applied load. The stress redistribution during creep was also highlighted for both load  
365 situations during stages 1 and 2. This in agreement with other studies led on different  
366 applications [16-19]. In the case of shear load, a closer study of the measured displacements  
367 allowed determining large differences for the out-of-plane displacement. This seems to indicate  
368 that there may be an anisotropic behaviour of the adhesive that is not currently taken into  
369 account in the modelling. Additional investigations are under progress to improve Burgers  
370 parameters identification, and study the possible implementation of anisotropic creep  
371 behaviour for stages 1 and 2. There is also a strong need for a model that would consider  
372 stage 3 to be able to model entirely creep process of such a bonded assembly [20].

373

## 374 **7. References**

375 [1] Court JP, Bonded assembly and bonding method, Patent WO2017089668 (A1). 2017.

376 [2] Hashim SA. Adhesive bonding of thick steel adherends for marine structures. *Mar Struct.*  
377 1999; 12:405-423. [https://doi.org/10.1016/S0951-8339\(99\)00029-5](https://doi.org/10.1016/S0951-8339(99)00029-5).

378 [3] Kinloch AJ. The science of adhesion – Part 2: Mechanics and mechanisms of failure. *J of*  
379 *Mat Sci* 1982; 17:617-651.

380 [4] Godzimirski J, Roskowicz M. Numerical analysis of long-lasting strength of adhesive bonds.  
381 *Adv in Manuf Sci and Tech* 2004; 28(1):67–83.

- 382 [5] Weitzenböck J.R. Adhesives in marine engineering, Woodhead Publishing Limited,  
383 Cambridge, 2012.
- 384 [6] Al-Ghamdi A. Fatigue and creep of adhesively bonded joints. Phd Thesis, Loughborough  
385 University, 2004.
- 386 [7] Broughton W. Creep testing of adhesive joints analysis of creep rupture data. Technical  
387 report, NPL; 1999.
- 388 [8] Cognard JY, Creach'cadec R, Maurice J, 2011. Numerical analysis of the stress distribution  
389 in single-lap shear tests under elastic assumptions – application to the optimisation of the  
390 mechanical behaviour. Intern J of Adhes and Adhes 2011, 31:715-724.  
391 <https://doi.org/10.1016/j.ijadhadh.2011.07.001>.
- 392 [9] Salençon J. Viscoélasticité pour le calcul des structures, l'École polytechnique Edition.  
393 Presse de l'École Nationale des Ponts et Chaussée, Paris ; 2016.
- 394 [10] Billon N, Bouvard JL. Propriétés et comportement mécanique des polymères  
395 thermoplastiques. Techniques de l'Ingénieur, AM3115; 2015.
- 396 [11] Penny RK, Mariott DL. Design for creep, McGraw-Hill, London; 1971.
- 397 [12] Da Silva LFM, Oschner A, Adams RD. Handbook of adhesion technology, Springer; 2011.
- 398 [13] Dean G, Urquhart J, Roberts S. Modelling creep in toughened epoxy adhesives for finite  
399 element analysis. Proceedings of Ninth Intern conf on the sci and tech of adhes and adhes,  
400 Oxford; 2005.
- 401 [14] Thai M. Modélisation micromécanique et simulation numérique du fluage des bétons avec  
402 prise en compte de l'endommagement et des effets thermo-hydriques. Ph.D. thesis, Université  
403 Paris-Est; 2012.
- 404 [15] Cognard J, Sohier L, Creac'hcadec R, Lavelle F, Lidon N. Influence of the geometry of  
405 coaxial adhesive joints on the transmitted load under tensile and compression loads. Intern J  
406 of Adhes and Adhes 2012; 37:37–49. <https://doi.org/10.1016/j.ijadhadh.2012.01.013>.
- 407 [16] Roy S, Reddy JN, 1986. Nonlinear viscoelastic analysis of adhesively bonded joints.  
408 Research report N0 VPI-E-86-28; Virginia Tech centre for adhesion science; 1986.

- 409 [17] Su N, Mackie RI. Two-dimensional creep analysis of structural adhesive joints. Intern J of  
410 adhes and adhes 1992; 13(1): 33-40. [https://doi.org/10.1016/0143-7496\(93\)90006-U](https://doi.org/10.1016/0143-7496(93)90006-U).
- 411 [18] Houhou N, Benzarti K, Quiertant M, Chataigner S, Flety A, Marty C. Analysis of the non-  
412 linear creep behaviour of FRP-concrete bonded assemblies. J of Adhes and Sci Tech 2014;  
413 29(14-15):1345-1366.
- 414 [19] Reza A, Shishesaz M, Naderan-Tahan K, 2014. The effect of viscoelasticity on creep  
415 behaviour of double-lap adhesively bonded joints. Lat Am J of solids and struct 2014; 11:35-  
416 50.
- 417 [20] Zehsaz M, Vakili-Tahami F, Saeimi-Sadigh MA, 2014. Parametric study of the creep failure  
418 of double lap adhesively bonded joints. Mat and Des 2014; 64:520-526.
- 419

**Fig. 1:** Photo of the solution developed by Cold Pad (application disposal on the left and adhesively bonded fastener on the right).

**Fig. 2:** Creep stages.

**Fig. 3:** Rheological creep models.

**Fig. 4:** Photo of studied C-Claw<sub>TM</sub> steel fastener T on the left and S on the right.

**Fig. 5:** Scheme of the two tested solicitation modes: Tension and Shear loadings.

**Fig. 6:** Protocol of the tensile creep test.

**Fig. 7:** Protocol of shear creep test.

**Fig. 8:** Measured displacements during tensile creep investigations at  $T = 25^{\circ}\text{C}$

**Fig. 9:** Creep shear at  $T = 25^{\circ}\text{C}$ .

**Fig. 10:** Scheme of the studied 2D axisymmetric model.

**Fig. 11:** Stress results obtained through finite element along the radius in the middle of the adhesive layer for different mesh sizes in tension.

**Fig. 12:** 3D model in tension.

**Fig. 13:** Boundary conditions for the shear model.

**Fig. 14:** Stress state for 2D axisymmetric model in tension.

**Fig. 15:** Comparison of the 2D and 3D model in tension.

**Fig. 16:** Stress state along the adhesive for the shear model.

**Fig. 17:** Redistribution of Von Mises stress for tensile model.

**Fig. 18:** Redistribution of Von Mises stress for the shear model.

**Fig. 19:** Experimental and numerical comparison of out-of-plane displacement for tensile creep test at  $25^{\circ}\text{C}$ .

**Fig. 20:** Experimental and numerical comparison of creep displacements (in-plane and out-of-plane) for shear test at 59 % and  $25^{\circ}\text{C}$ .

**Fig. 21:** Experimental and numerical comparison of creep displacements (in-plane and out-of-plane) for shear test at 67 % and  $25^{\circ}\text{C}$ .



**Fig. 1:** Photo of the solution developed by Cold Pad (application disposal on the left and adhesively bonded fastener on the right)

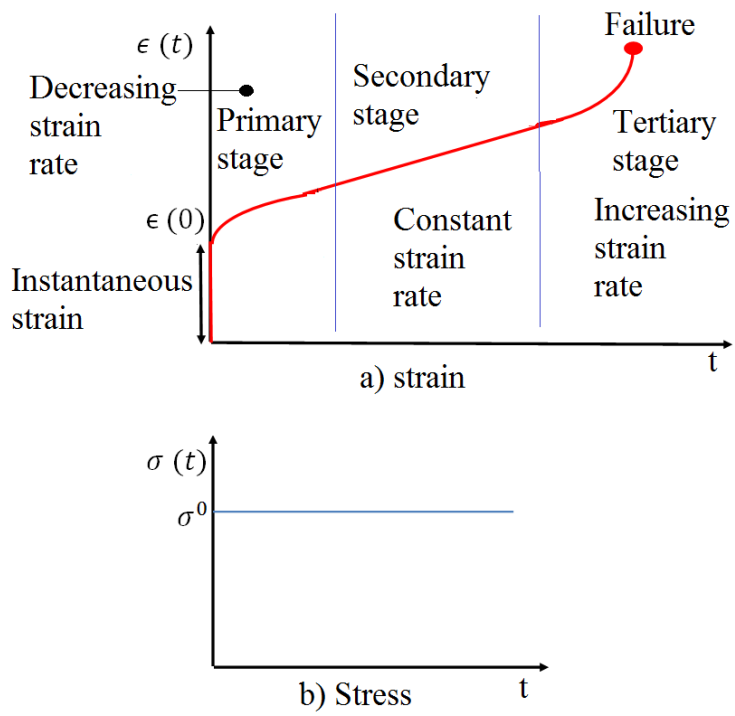


**Fig. 2:** Creep stages.

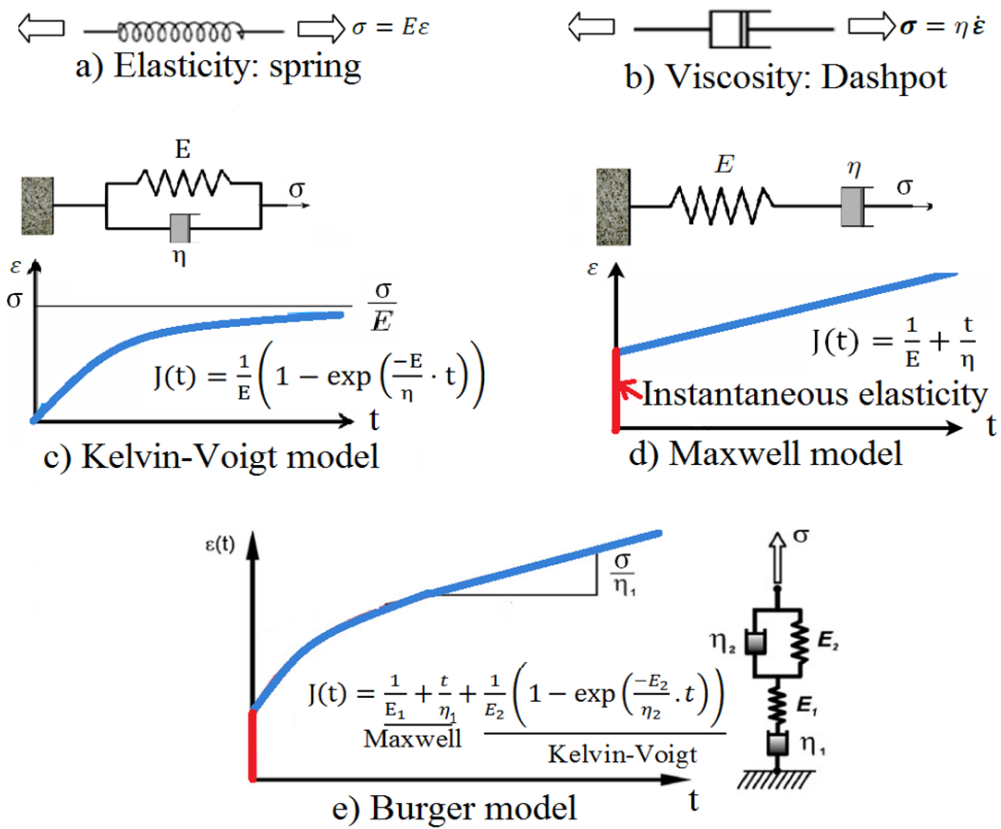


Fig. 3: Rheological creep models.



**Fig. 4:** Photo of studied C-Claw<sup>TM</sup> steel fastener T on the left and S on the right.



**Fig. 5:** Scheme of the two tested sollicitation modes: Tension and Shear loadings.

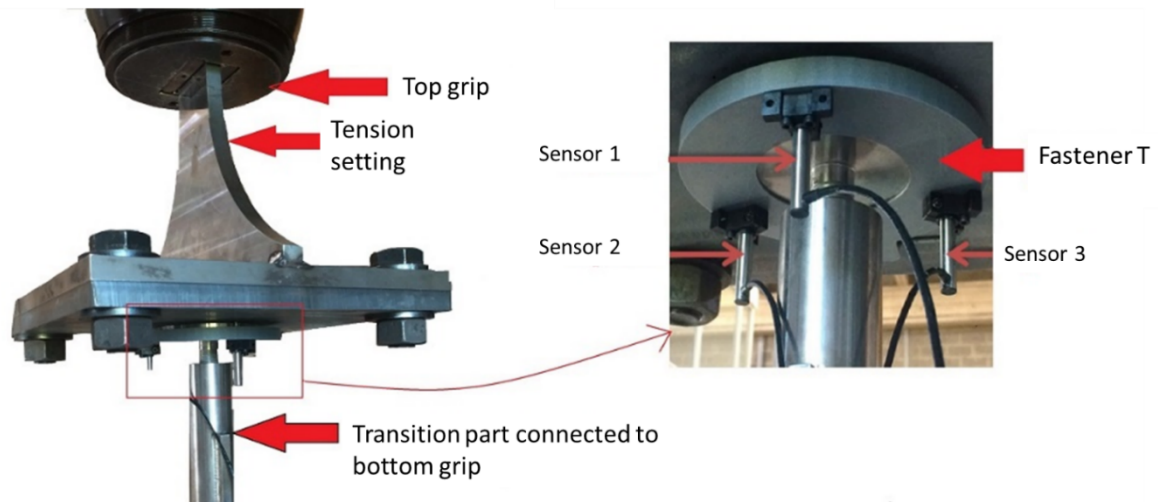


**Fig. 6:** Protocol of the tensile creep test.

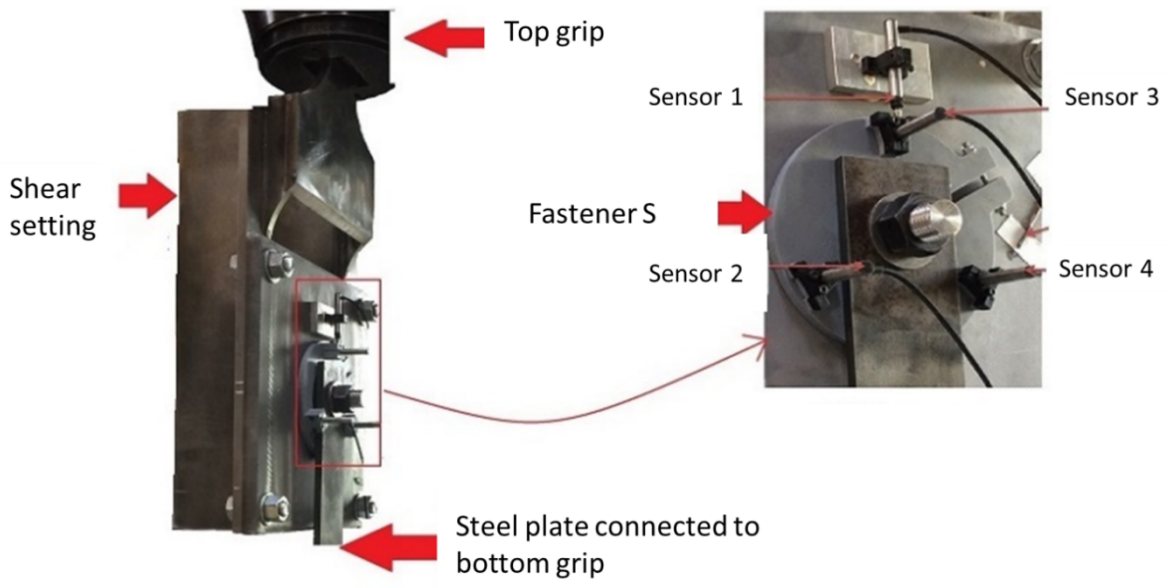
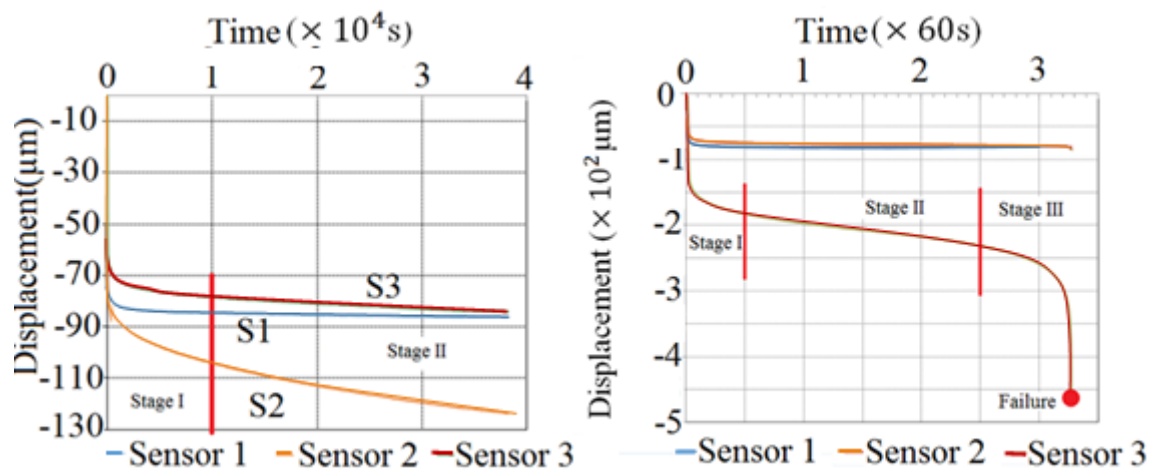


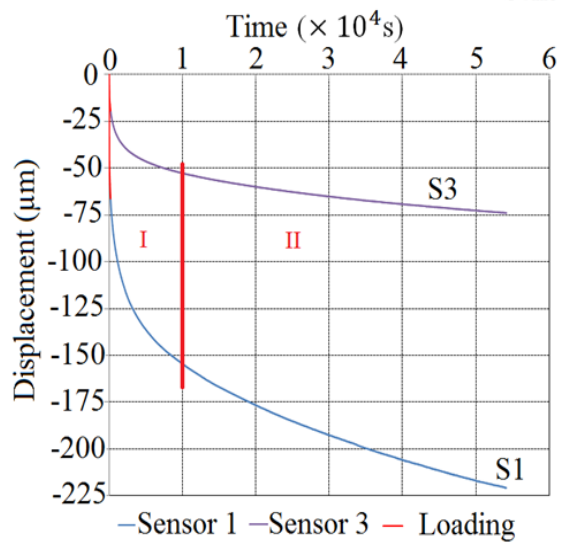
**Fig. 7:** Protocol of shear creep test.



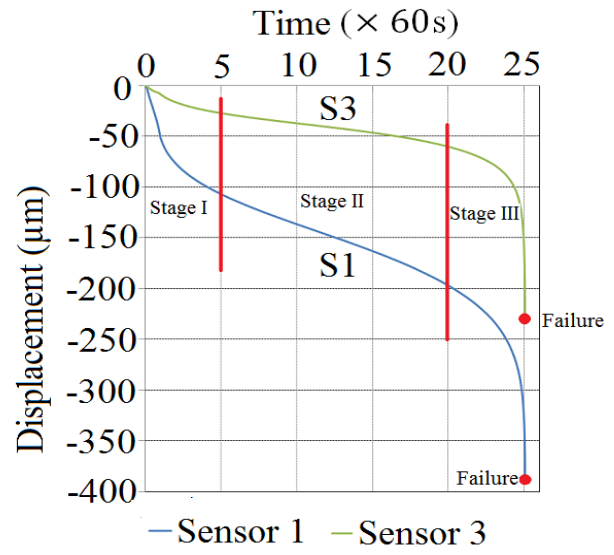
a) 59 %  $T_{\text{ult}}$

b) 69 %  $T_{\text{ult}}$

**Fig. 8:** Measured displacements during tensile creep investigations at  $T = 25^{\circ}\text{C}$



a) 59 % S ult



b) 67 % S ult

**Fig. 9:** Creep shear at  $T = 25^\circ\text{C}$ .

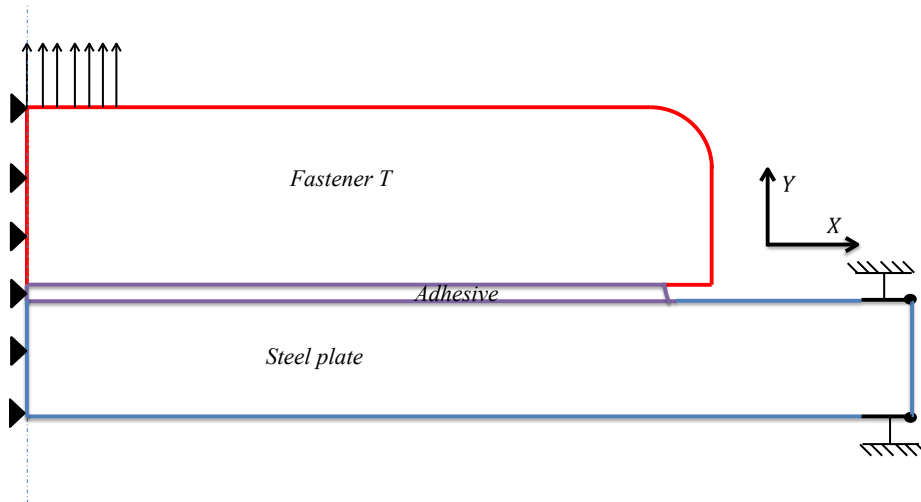


**Fig. 10:** Scheme of the studied 2D axisymmetric model.

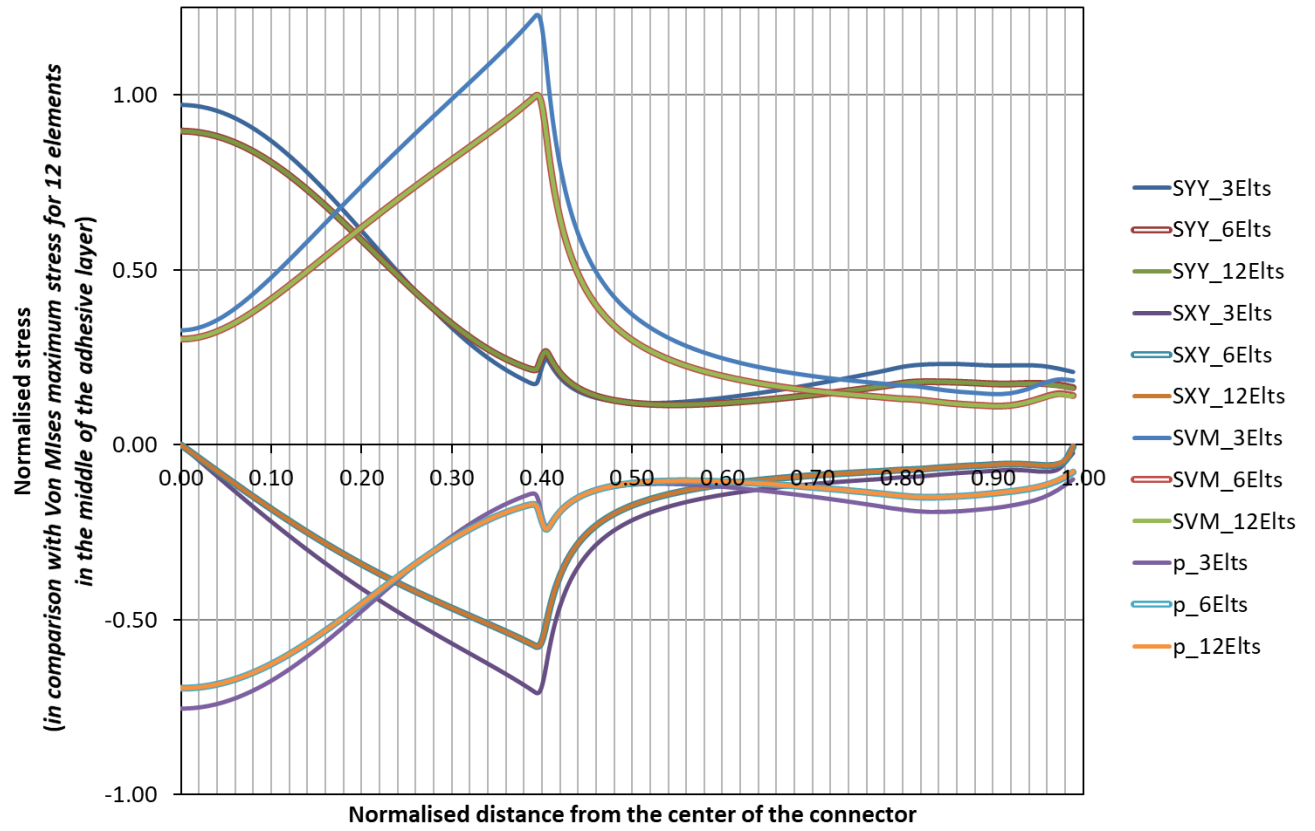


**Fig. 11:** Stress results obtained through finite element along the radius in the middle of the adhesive layer for different mesh sizes in tension

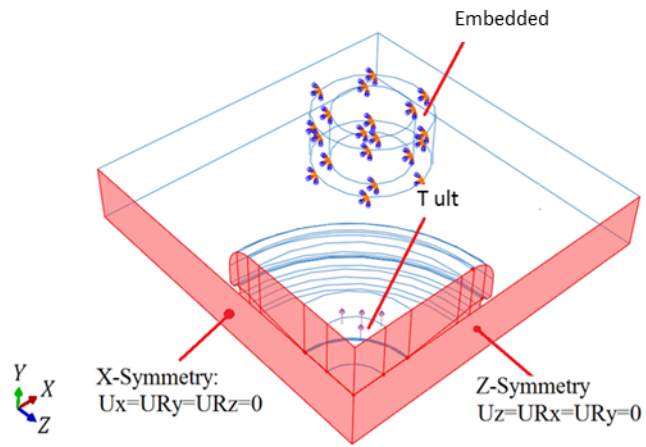


**Fig. 12:** 3D model in tension.

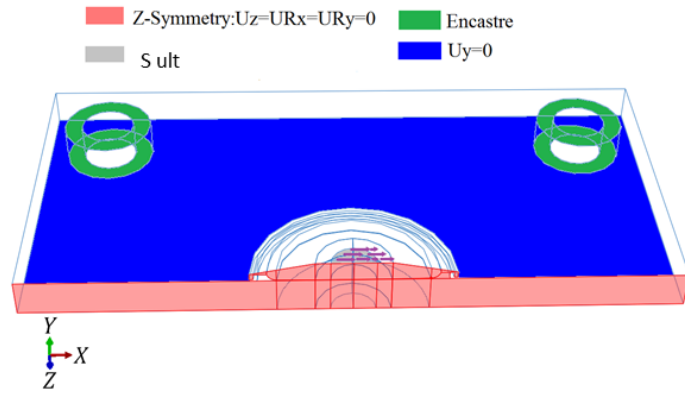


**Fig. 13:** Boundary conditions for the shear model.

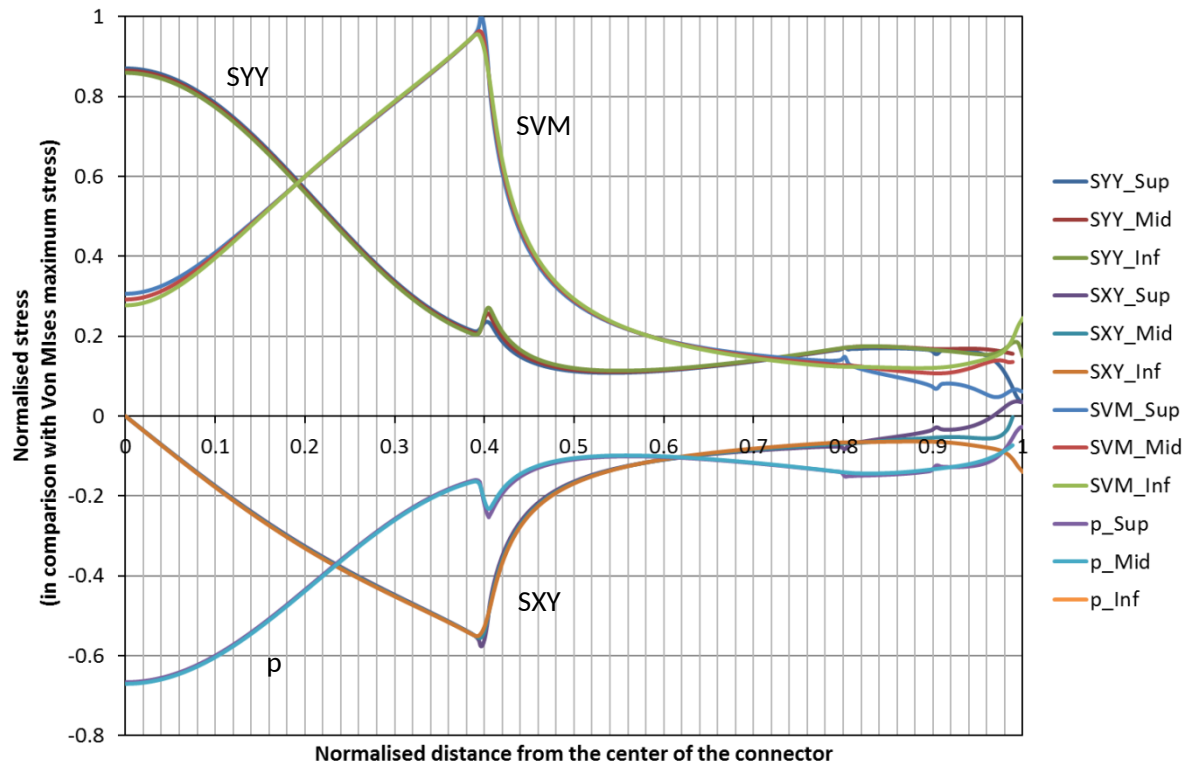
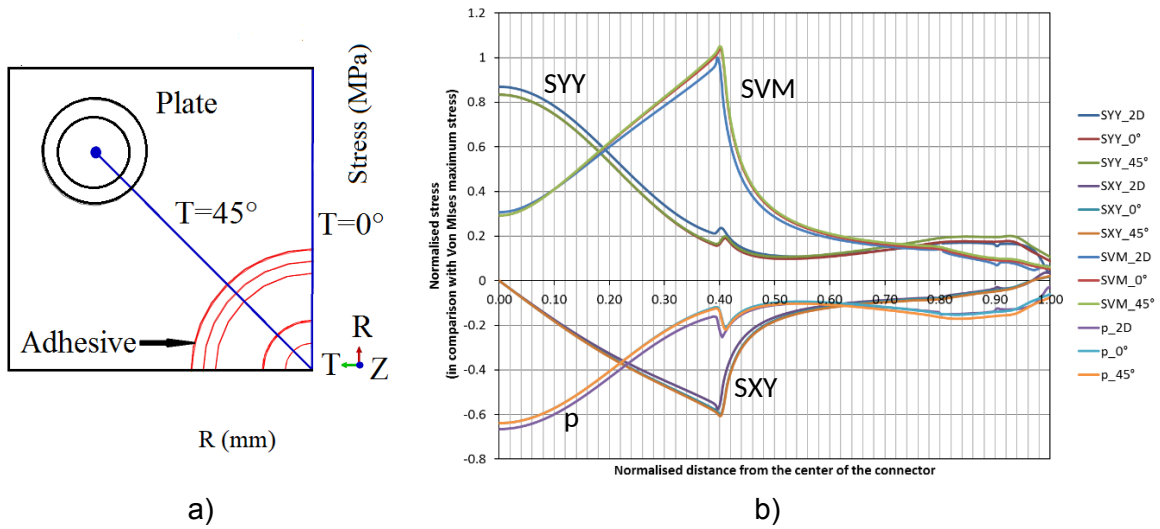


Fig. 14: Stress state for 2D axisymmetric model in tension.



**Fig. 15:** Comparison of the 2D and 3D model in tension.

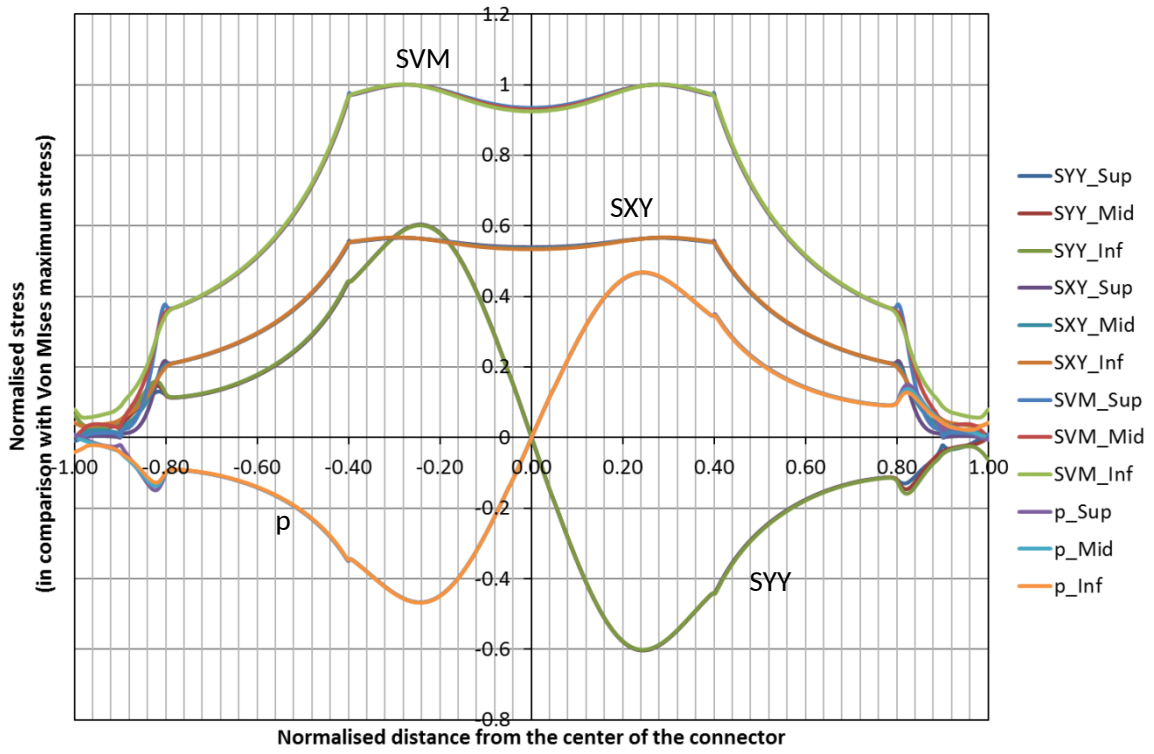
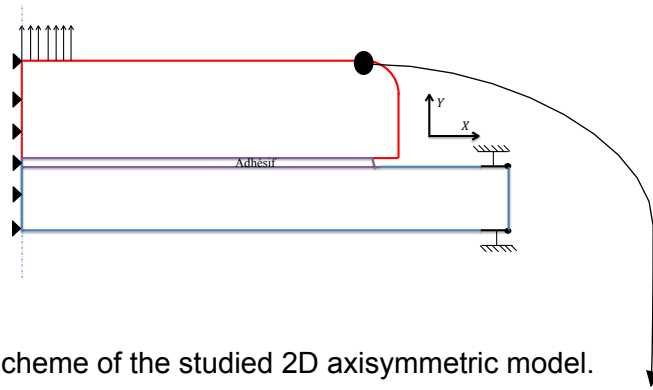
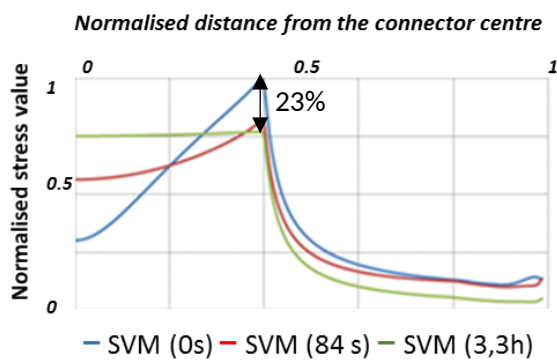


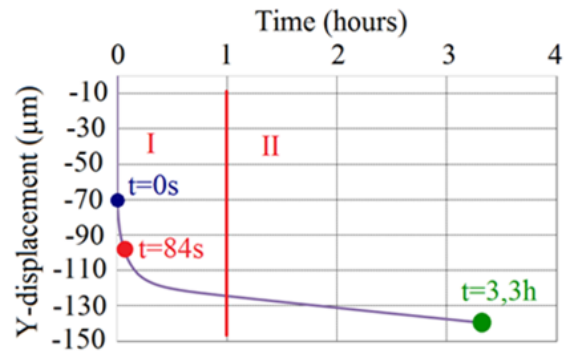
Fig. 16: Stress state along the adhesive for the shear model.



a) Scheme of the studied 2D axisymmetric model.

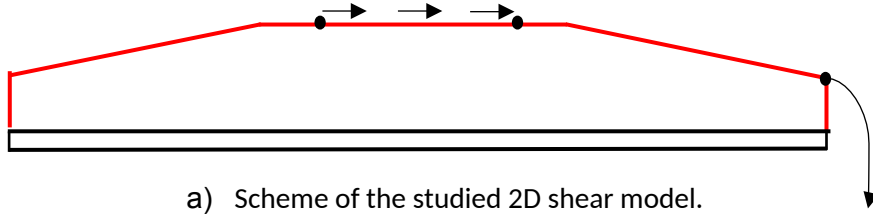


b) Stress redistribution

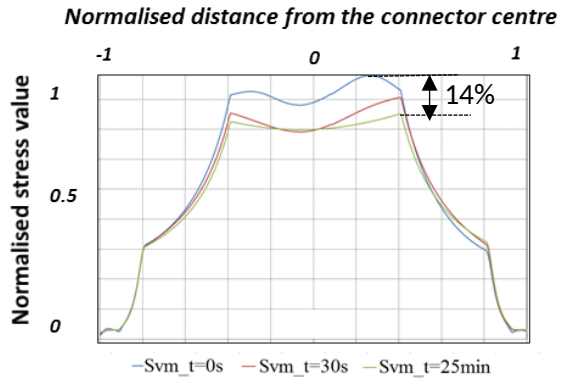


c) Creep displacement

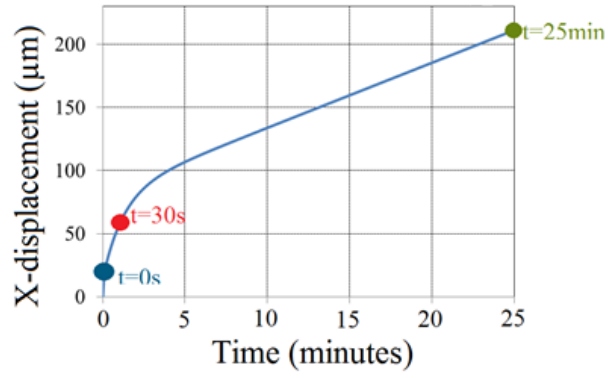
Fig. 17: Redistribution of von Mises stress for tensile model.



a) Scheme of the studied 2D shear model.



b) Stress redistribution



c) Creep displacement

**Fig. 18:** Redistribution of von Mises stress for the shear model.

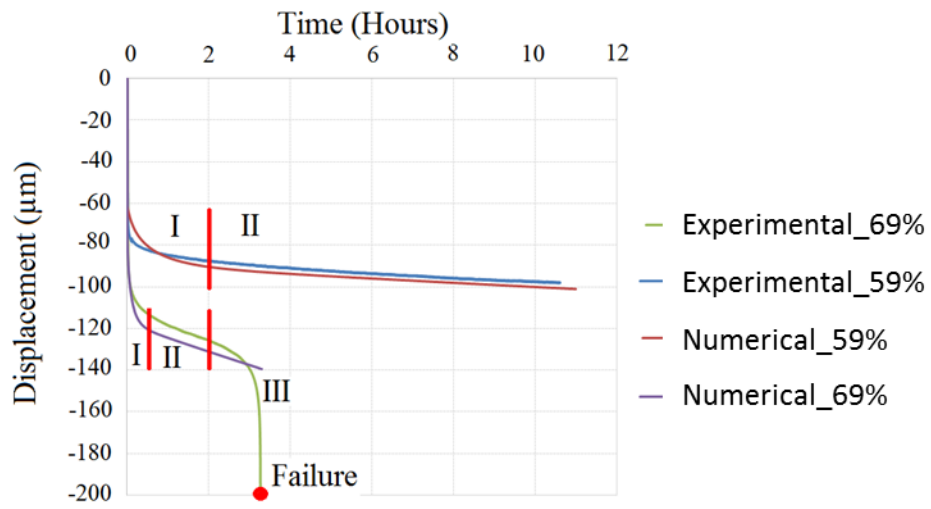
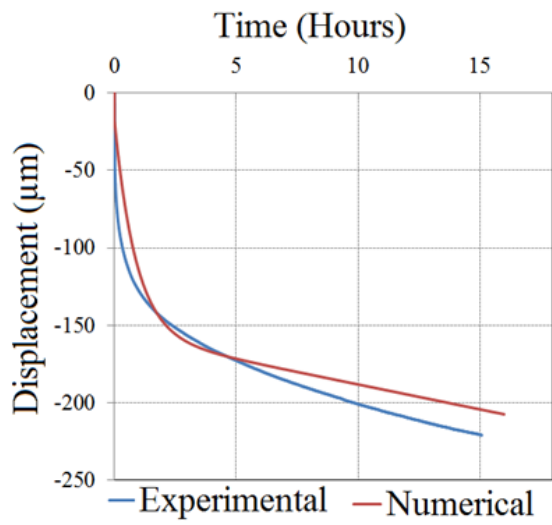
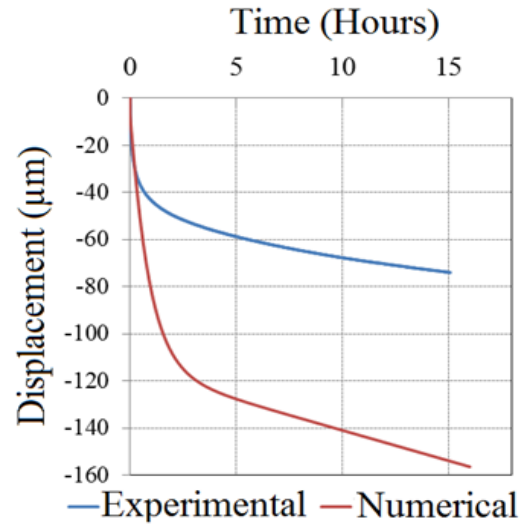


**Fig. 19:** Experimental and numerical comparison of out-of-plane displacement for tensile creep test at 25°C.

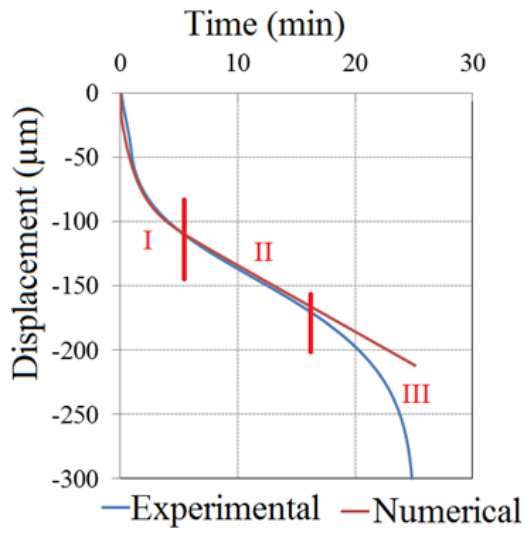


a) In-plane displacement (sensor 1)

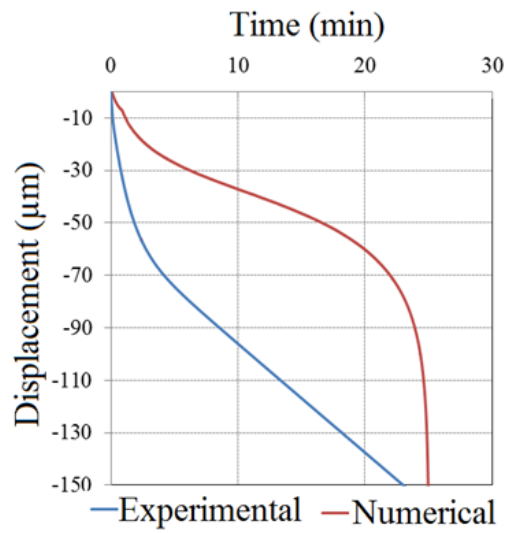


b) Out-of-plane displacement (sensor 3)

**Fig. 20:** Experimental and numerical comparison of creep displacements (in-plane and out-of-plane) for shear test at 59 % and 25°C.



a) In-plane displacement (sensor 1)



b) Out-of-plane displacement (sensor 3)

**Fig. 21:** Experimental and numerical comparison of creep displacements (in-plane and out-of-plane) for shear test at 67 % and 25°C.

**Table 1:** Characteristics of the tested adhesive provided by the supplier

$E$ (MPa)	$RT$ (MPa)	$Tg$ (°C)
1200-1700	22-24	80

**Table 2:** Burger's law parameters

Applied load	$E_1$ (MPa)	$\eta_1$ (MPa.h)	$E_2$ (MPa)	$\eta_2$ (MPa.h)
Tension (59%)	1200	5000	400	300
Tension (69%)	1200	750	220	30
Shear (59%)	1200	1700	40	35
Shear (67%)	1200	19.83	100	2.083